Hybridized orbital states in spin-orbit coupled $3d-5d$ double perovskites studied by x-ray absorption spectroscopy

Min-Cheol Lee,[1,2] Sanghyun Lee,[3] C. J. Won,[4] K. D. Lee,[4] N. Hur,[4] Jeng-Lung Chen,[5] Deok-Yong Cho,[6,*] and T. W. Noh[1,2]

[1]*Center for Correlated Electron Systems, Institute for Basic Science, Seoul 08826, Republic of Korea*

[2]*Department of Physics and Astronomy, Seoul National University, Seoul 08826, Republic of Korea*

[3]*Institute of Material Structure Science, KEK, Tokai 319-1106, Japan*

[4]*Department of Physics, Inha University, Incheon 22212, Republic of Korea*

[5]*National Synchrotron Radiation Research Center, Hsinchu 30076, Taiwan*

[6]*IPIT and Department of Physics, Chonbuk National University, Jenju 54896, Republic of Korea*

(Received 26 December 2017; revised manuscript received 2 March 2018; published 15 March 2018)

We investigated the orbital hybridization mechanism in $3d-5d$ double perovskites (DPs) of La_2CoIrO_6 and La_2CoPtO_6 using x-ray absorption spectroscopy. It is clearly evidenced by O K-edge and Co K-edge x-ray absorption spectra that the Co $3d$ orbitals hybridize not only with the half-filled Ir/Pt $j_{\rm eff}$ states but also with the fully empty (unpolarized) Ir/Pt e_g states in both DPs. The Co $3d$ e_g-Ir $5d$ e_g hybridization cannot contribute to the ferrimagnetic long-range order in La_2CoIrO_6 established by spin-selective Co $3d$ t_{2g}-Ir $5d$ $j_{\rm eff}$ hybridization through the intermediate oxygen p state but could serve as an origin of paramagnetism. The strengths of such orbital hybridizations were found to be almost invariant to temperature, even far above the Curie temperature, implying persistent paramagnetism against the antiferromagnetic ordering in the spin-orbit entangled $3d-5d$ DPs.

DOI: 10.1103/PhysRevB.97.125123

I. INTRODUCTION

Transition-metal (TM) perovskite oxide is a fundamental platform for studying various electronic and magnetic phenomena in condensed matter, driven by the spin, orbital, lattice, and the coupling between them. In the perovskite framework of ABO_3 (A = rare-earth ion and B = TM ion), the d orbital states in the B site are split up into triplet t_{2g} and doublet e_g states due to the octahedral crystal field [1,2], and the filling and the energetics of the two manifolds play the most significant roles in determining the electronic properties of the material. Hence, it is important to understand the detailed mechanisms of interactions among the d electrons, which include both the interatomic and intra-atomic interactions.

One plausible way to examine the intersite interactions is to utilize a double perovskite (DP). A DP has a formula of $A_2BB'O_6$ (A = rare earth element, B/B' = TM ions) with structures of alternating B and B' sublattices, namely, with a three-dimensional checkerboard-type arrangement. The schematics of the BO_6 octahedron in perovskites and $BO_6-B'O_6$ octahedral unit in DPs are depicted in Figs. 1(a) and 1(b), respectively. For instance, in an iridate DP, La_2CoIrO_6, the spin moments of the B(Co) and B'(Ir) sublattices are distinguishable, so that one can examine the spin structures of each atomic species as depicted in Fig. 1(c). In general, the spins at the B and B' sites in DPs prefer to be ordered either ferromagnetically or antiferromagnetically depending on the detailed energetics of intersite spin-spin interactions [3–6]. For some DPs, including a representative $3d-4d$ DP of Sr_2FeMoO_6 [4] or a $3d-5d$ DP of Sr_2CrOsO_6 [5,6], the spins at the B and B' sites are ordered antiparallel to show a strong ferrimagnetism with high Curie temperatures [5–8]. It is well known that such magnetic ordering can be explained by the mechanism of intersite orbital hybridizations [3–7].

In this work, we focus on the characterization of iridate and platinate DPs among $3d-5d$ DPs to reveal the complex interplay of the $3d-5d$ orbital hybridizations. Recently, $5d$ compounds, including iridates [9–11] and osmates [12,13], have been extensively studied to scrutinize the atypical quantum basis of $J_{\rm eff}$ states [9,11], which is now acknowledged to be a physical platform for exotic phenomena, including the relativistic Mott insulating phase [9,10] and the quantum spin liquid phase according to the Kitaev model [11,14]. In addition, fabrication of iridate [15–21], osmate [22–25], and rhenate [26] DPs has been reported to date. In many cases, the specimens were designed to have partial occupancies in the spin-orbit coupled $J_{\rm eff}$ states, namely, with Ir^{4+} (d^5), Os^{5+} (d^3), or Re^{6+} (d^1), to study the inherently coupled nature of spin-orbit (SO) entangled states. Due to the interplay of strong SO coupling and crystal field, a good quantum number of a $5d$ electron should be $j_{\rm eff} = l_{\rm eff} \oplus s = 1 \pm 1/2$ rather than the respective $l = 2$ or $s = 1/2$ [9]. As in many other $5d$ oxides, the SO coupling will split the t_{2g} manifolds further into a fourfold $j_{\rm eff} = 3/2$ and a doublet $j_{\rm eff} = 1/2$ in the $5d$ DPs, as shown in the right panel of Fig. 1(a).

Nevertheless, the fundamental question about the influence of the spin-orbit coupled $J_{\rm eff}$ states on the magnetism has not been answered yet. Therefore, it is timely to examine the orbital hybridizations in the iridate DPs and relatively new platinate DP experimentally. Some earlier studies have

*Corresponding author: zax@jbnu.ac.kr

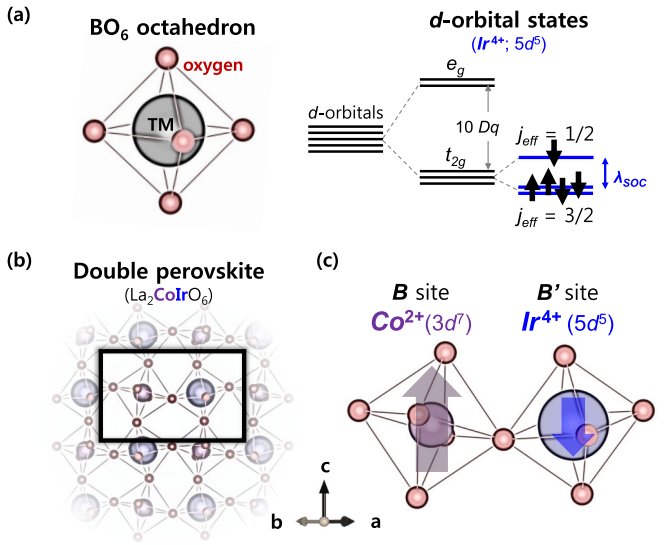

FIG. 1. (a) The BO_6 octahedron (B = TM cation) with the energy split for d-orbital states according to the octahedral crystal field ($10Dq$) with an additional large spin-orbit coupling λ_{SOC} in the case of Ir^{4+} ($5d^5$). (b) Simplified picture of alternating ordering of Co^{2+} (purple) and Ir^{4+} (blue) with intervening O^{2-} (red) in an $A_2BB'O_6$ DP, e.g., La_2CoIrO_6. The solid black box shows a single pair of BO_6–$B'O_6$ for clarity. (c) Antiferromagnetic coupling of spins between B (Co^{2+}) and B' (Ir^{4+}) in the case of La_2CoIrO_6. Spin-selective intersite hybridization between the adjacent cations through the oxygen orbital states stabilizes the antiferromagnetic alignments of spins (colored arrows).

verified a ferrimagnetic ground state in La_2CoIrO_6 with an antiferromagnetic coupling between the $3d$ Co and $5d$ Ir sublattices [15–17]. Particularly, recent x-ray absorption spectroscopy studies [16,17] further confirmed the spin states of the sublattices, Co^{2+} ($3d^7$ high spin; $S = 3/2$) and Ir^{4+} ($5d^5$; $j_{\rm eff} = 1/2$). It was also suggested that an A-site doping with Ca and Sr in La_2CoIrO_6 can suppress the magnetism due to valence changes in the Co and Ir ions [15,19]. In regard to magnetism, the Curie temperature of La_2CoIrO_6 is approximately $T_C = 95$ K [16–18], much lower than those in other $3d$–$5d$ DPs such as Sr_2CrReO_6 (635 K) [27] and Sr_2CrOsO_6 (725 K) [6]. In addition, a platinate DP La_2CoPtO_6, where Pt^{4+} ($5d^6$; $S = 0$) is nonmagnetic with fully occupied t_{2g} states, shows much weaker magnetism with $T_C < 50$ K [17]. To address why the magnetic orders are weaker in the iridate and platinate DPs, we elucidated the orbital hybridization mechanism for stabilization of the magnetic order based on the results of x-ray spectroscopies.

We used x-ray absorption spectroscopy (XAS) to observe the hybridized orbital states in the iridate and platinate DPs experimentally. Due to the strict selection rule in the XAS process, exact information from specific orbital states can be deduced. For instance, in O K-edge XAS, Co $3d$ and Ir/Pt $5d$ orbital states hybridized with O $2p$ were captured, while in Co K-edge XAS, Co $4p$ states hybridized with Ir/Pt $5d$ e_g were captured. Detailed analyses of the XAS data revealed that the magnetism in the DPs can be explained in terms of the inherent nature of the spin-orbit entangled $J_{\rm eff}$ states as well as the abundance of hybridized orbital states of Ir/Pt $5d$-Co $3d$ (and $4p$) states.

II. EXPERIMENTAL DETAILS

A. Sample preparation

The polycrystalline La_2CoIrO_6 (La_2CoPtO_6) powder was prepared via solid-state syntheses of a stoichiometric mixture of La_2O_3, Co_3O_4, and IrO_2 (PtO_2), as described in earlier work [17]. The polycrystalline La_2NiIrO_6 (La_2ZnIrO_6) was prepared using the same method, except that NiO (ZnO) was used to replace Co_3O_4. All the samples were confirmed to be in crystallographically single phases by x-ray diffraction measurement.

B. X-ray absorption spectroscopy

O K-edge XAS was conducted at the 2A beamline of the Pohang Light Source in total-electron-yield mode. Hard x-ray absorption spectroscopy at the Co K and Ir/Pt L_3 edges was performed at the 17C1 beamline of the Taiwan Light Source in transmission yield mode. The specimens were cooled down to 19 K first, and the temperature-dependent data were collected with increasing temperature. The specimens were prepared in thin pelletized forms to minimize the contribution from voids or inhomogeneity in mass density. The polarization of the incident x rays was set to be parallel to the pellet plane for all the measurements. All the XAS data were normalized by the edge jumps after subtracting small background slopes below and above the edges. The simulation of the x-ray absorption near-edge structure (XANES) was processed using the *ab initio* multiple-scattering code FEFF8 [28]. A full multiple scattering within a distance of 6 Å from the central atom is considered. The lattice constants and atomic coordinates were taken from the results of the neutron diffraction study. The local density of states (LDOS) of Ir or Pt was calculated in the same manner (FEFF8) but taking the LDOSs from all the Ir or Pt atoms other than the central atom to minimize the core-hole effects.

III. RESULTS

A. O K-edge XAS

It is confirmed with O K-edge XAS that the electronic structure of the $3d$–$5d$ DPs near the chemical potential is dominated by $5d$ $j_{\rm eff}$ hybridized orbital states with a relatively small contribution from $3d$ states. Figure 2(a) shows the O K-edge XAS spectra from the three iridate DPs La_2CoIrO_6, La_2NiIrO_6, and La_2ZnIrO_6 obtained at a temperature T of 300 K. The spectra near the threshold represent transitions from O $1s$ core levels to unoccupied O $2p$ states, which are hybridized with orbital states from the TM ions [29,30]. As shown in Fig. 2(a), the difference in B ions (Co, Ni, and Zn) does not affect the overall line shapes of the spectra significantly. Moreover, an x-ray photoemission spectroscopy (XPS) study confirmed that all the B cation valences were mostly +2 regardless of the atomic species, i.e., Co^{2+} ($3d^7$), Ni^{2+} ($3d^8$), and Zn^{2+} ($3d^{10}$), and the Ir valences remained +4 for all three DPs (not shown). Therefore, the similar resonant energies and intensities in the O K-edge spectra suggest that the unoccupied electronic structures are dominated by the Ir

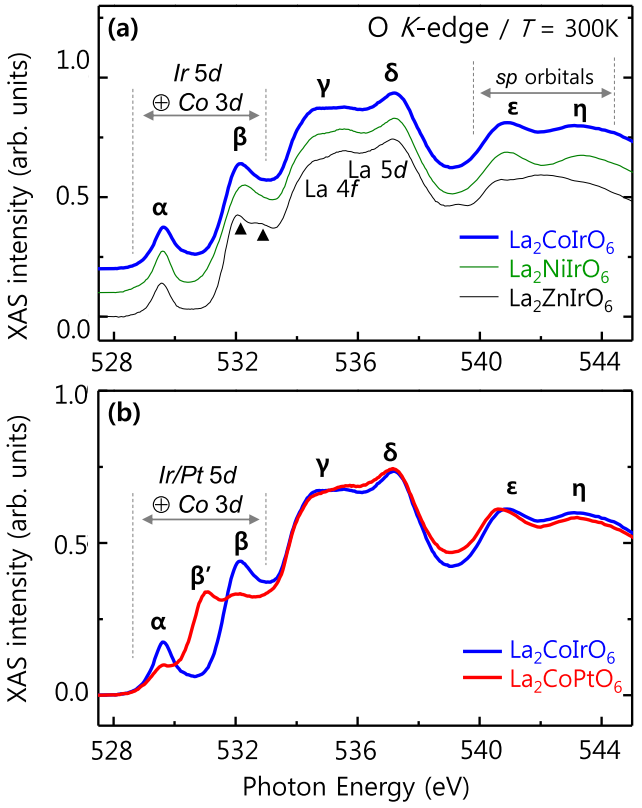

FIG. 2. The O K-edge XAS spectra of (a) La_2CoIrO_6, La_2NiIrO_6, and La_2ZnIrO_6 and (b) La_2CoIrO_6 and La_2CoPtO_6. Peaks α, β, and β' are attributed to the d-orbital states of the transition-metal (TM) ions, including Ir/Pt $5d$ and Co (or Ni) $3d$, while γ and δ are attributed mainly to the La $4f$ and $5d$ orbital states, respectively. Peaks ϵ and η can be attributed to the sp orbital states from all the cations.

$5d$ states. As a result, peaks α and β in Fig. 2(a) should be attributed mostly to the unoccupied Ir $j_{\rm eff} = 1/2$ and Ir e_g states under octahedral crystal field.

Besides the overall similarity in the O K-edge spectra, additional contributions from the $3d$ orbitals were also observed. In the case of La_2ZnIrO_6, the low-energy peaks can be attributed only to Ir^{4+} $5d$ orbitals because the Zn $3d$ shell in Zn^{2+} is completely filled (d^{10}). Thus, an apparent 0.7 eV split in peak β highlighted by the triangles in Fig. 2(a) should be attributed to some changes in $5d$ orbital states in Ir^{4+}. The most plausible reason for the split is an additional crystal field effect in the e_g state due to lowering of local symmetry in the IrO_6 octahedron. In contrast to La_2ZnIrO_6, the β doublet appears to merge in the cases of La_2CoIrO_6 and La_2NiIrO_6. This is seemingly caused by the emergence of the unoccupied $3d$ e_g states in Co^{2+} (d^7) or Ni^{2+} (d^8) near $h\nu \sim 532$ eV. The unoccupied Co e_g states are also observed in the case of La_2CoPtO_6 as a shoulder peak near the same energy in Fig. 2(b).

In addition, peak α exhibits a small higher-energy shoulder ($h\nu \sim 530$ eV), particularly in the case of La_2CoIrO_6. This can be attributed to the unoccupied $3d$ t_{2g} state of Co^{2+} (d^7), while there should not be such effects from the fully occupied t_{2g} orbitals in Ni^{2+} (d^8) and Zn^{2+} (d^{10}).

Hence, the O K-edge XAS spectra suggest that the electronic structure near the chemical potential in the three iridate DPs is dominated by the Ir $5d$ $j_{\rm eff} = 1/2$ states, with a relatively small contribution from B (Co or Ni) $3d$ states. Specifically, a stronger orbital hybridization in Ir $5d$-O $2p$ might be responsible for the greater intensity of the $5d$ signals over the $3d$ ones. The relatively dispersive nature of the $5d$ orbitals in comparison to the $3d$ orbitals would enhance the hybridization strengths with oxygen $2p$ orbitals.

To investigate how the $5d$ TM ions change the electronic structures in the DP system, we additionally performed XAS on a platinate DP, La_2CoPtO_6. Note that Pt^{4+} in the platinate DP has one more electron than Ir^{4+} in iridate DPs. Thus, the $j_{\rm eff} = 1/2$ states in La_2CoPtO_6 are fully occupied by electrons (Pt^{4+}; $5d^6$) with total spin $S = 0$. For comparison, the O K-edge XAS spectra from both La_2CoIrO_6 and La_2CoPtO_6 are plotted in Fig. 2(b). The two spectra appear to be very different from each other at $h\nu$'s below 534 eV but are quite similar at $h\nu$'s above 534 eV. This suggests that the higher-energy peaks (γ,δ,ϵ, and η) should originate from the orbital states less dependent on the replacement of the TM ion (from Ir to Pt). Peaks γ and δ are attributed to La $4f$ and $5d$ orbital states, and ϵ and η are attributed to the sp orbital states from all of the cations. Meanwhile, peaks α, β, and β' are attributed mainly to the Ir/Pt d-orbital states of Ir/Pt $j_{\rm eff} = 1/2$, Ir e_g, and Pt e_g, respectively.

In the spectrum of La_2CoPtO_6 [Fig. 2(b)], an additional peak is observed near $h\nu = 532$ eV. This can be attributed to the unoccupied Co $3d$ e_g states in the platinate. Note that this feature is irrelevant to β', which is the hybridized state of occupied Co e_g and unoccupied Pt e_g. In particular, peak α is also observed at the lowest energy (529.6 eV), even in the case of La_2CoPtO_6, suggesting the presence of the Co $3d$ t_{2g} state and its contribution to peak α.

B. Co K-edge and Ir/Pt L-edge XANES

To investigate the electronic structures of the iridate and platinate DPs further, hard x-ray absorption spectroscopy was also performed at the Co K edge and Ir/Pt L_3 edge. Figure 3 shows the Co K-edge XAS spectra of La_2CoIrO_6 and La_2CoPtO_6 powders at $T = 297$ K. The Co K-edge XAS spectra predominantly reflect the electric dipole transitions from the Co $1s$ core level to the Co p continuum state. Namely, the near-edge spectra reflect mostly the Co $4p$ states. Overall, the XAS results of the two specimens [Fig. 3(a)] coincide with each other. In general, x-ray absorption fine structures (XAFSs) after the absorption threshold are determined by local arrangements of atoms neighboring the photon-absorbing atom [31,32]. Therefore, the coincidence of the XAS spectra strongly suggest nearly identical crystal structures despite the different electron numbers of the $5d$ TM ions.

For comparison, the results of FEFF8 simulations [32] are shown in Fig. 3(a) together with measured XAS data. The simulations were performed based on the crystal structures of the DPs ($P2_1/n$) [15,17]. Full multiple-scattering schemes were employed with confinement of the radius of atomic orders up to 6 Å. It is clear that the oscillatory features above the edge jump in the experimental spectra are almost perfectly reproduced by the theoretical calculations.

In contrast to the XAFS features above the transition threshold ($h\nu > 7720$ eV), the preedge features ($h\nu = 7710$–7718 eV) show clear distinctions between the DPs. Figure 3(b)

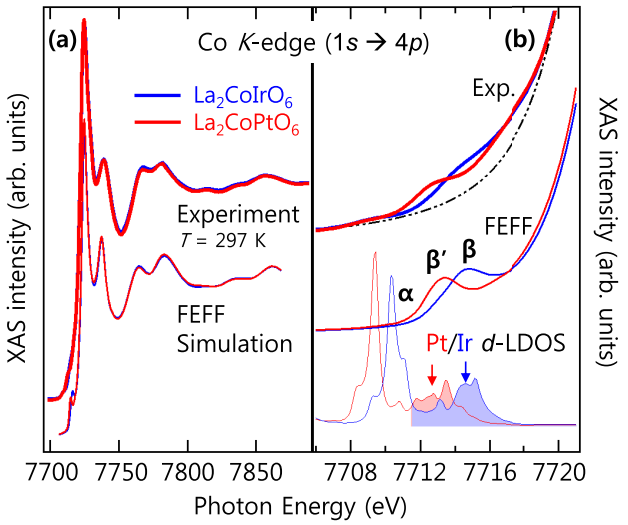

FIG. 3. (a) The Co K-edge XAS (Co $1s \rightarrow p$) spectra of La_2CoIrO_6 and La_2CoPtO_6 with the simulated spectra from FEFF8. (b) The enlarged view of the preedge regions with the Ir/Pt d local densities of states (LDOSs) obtained from FEFF8. The shaded regions highlight the correspondence to the peaks (β and β') in the experimental data. Peaks α, β, and β' correspond to those in Fig. 2. The presence of peaks β and β' evidently shows the effects of orbital hybridization between the Ir/Pt $5d$ and Co $4p$ orbitals.

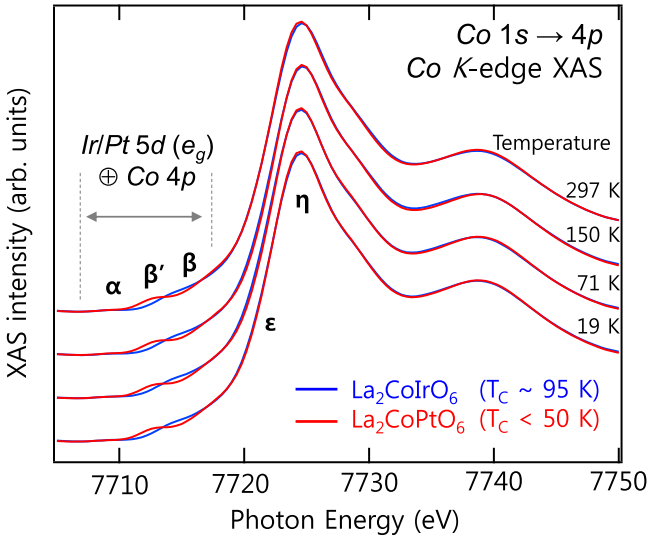

FIG. 4. T-dependent Co K-edge XANESs of La_2CoIrO_6 and La_2CoPtO_6. The features denoted by α to η coincide with those in Figs. 2 and 3(b). The preedge features (α, β, and β') are nearly independent of T even up to room temperature, suggesting that the Co $4p$-Ir/Pt $5d$ orbital hybridization should play a substantial role in determining the magnetic orders in the $3d-5d$ DP systems at T even far above the Curie temperature.

shows a magnified view of the preedge regions. Since the final states in the XAS process at the Co K edge should be the unoccupied Co $4p$, the presence of the preedge peaks below the main edge jumps evidently shows a partial electron filling of Co $4p$ via the intrasite mixing with occupied Co $3d$. In general, the preedge features are largely contributed by the d orbital states from either (i) the photon-absorbing atom itself (namely, Co $3d$) through the electric quadrupole transition ($E2$) or (ii) the nearby atoms (namely, Ir/Pt $5d$) through the $E1$ transition due to the nonlocal orbital hybridizations mediated by O $2p$ orbitals [33,34]. It is evident that the former contribution cannot properly explain the distinct preedge features because the Co electronic structures of the two systems have been found to be identical with a high-spin configuration [17]. Therefore, the preedge features should be attributed to nonlocal orbital hybridization between Ir/Pt $5d$ and Co $4p$ states via O $2p$ orbitals.

XAS simulation enabled concrete assignments of the preedge peaks. The simulated spectra from FEFF8 almost perfectly reproduced the preedge features, as shown in Fig. 3(b). The LDOSs for the Ir/Pt d states calculated from the simulation are also shown at the bottom of Fig. 3(b) with an arbitrary energy shift of +7708 eV. Although the FEFF8 simulation might not be accurate enough to describe the electronic structures of strongly correlated electron systems, it can represent rough approximations of the orders of the Ir/Pt d LDOS energies. Therefore, the LDOS peaks can clarify the orbital states relevant to the preedge peaks. The sharp LDOSs at lower energies correspond to the occupied $5d$ t_{2g} ($j_{\rm eff} = 3/2$ and 1/2) states, while those at higher energies highlighted by the shaded areas correspond to the unoccupied $j_{\rm eff} = 1/2$ (α) and Ir/Pt e_g (β/β') states. Peak α is absent in the preedge spectra because the hybridization between Co $4p$ and Ir/Pt $5d$ t_{2g} is not allowed due to bonding symmetry, which will be discussed further in the next section. These peak assignments are highly consistent with those in the O K-edge data in Fig. 2.

Figure 4 shows the Co K-edge XAS spectra of the two DPs obtained at a range of T's from 19 to 297 K. The main peaks and the preedge peaks are assigned labels from α to η to be consistent with Figs. 2 and 3. The XAS results above the edge energy are nearly identical for all T's, indicating that the atomic arrangements reflected in Co $4p$ hardly change with increasing T. Surprisingly, the preedge features of α, β, and β' are also almost constant with T up to room temperature, which is far above the Curie temperatures ($\lesssim$ 100 K). This strongly suggests that the hybridization between Co $4p$ and Ir/Pt $5d$ orbitals is strong enough to play a persistent role in determining magnetic orders in the $3d-5d$ DPs.

Figures 5(a) and 5(b) show the Ir/Pt L_3-edge XAS spectra of the La_2CoIrO_6 and La_2CoPtO_6 DPs with various T's, respectively. The XANESs showed no signature of a T evolution, again suggesting the stabilization of the hybridized orbital states. The robust electronic structure is in agreement with the negligible structural evolution with T below room temperature [15].

IV. DISCUSSION

A. Orbital hybridization in iridate and platinate DPs

In general, the origin of the magnetic ordering of cations in DPs can be understood by the mechanism of orbital hybridization [3,4]. This mechanism has successfully explained the magnetically ordered spin states in most DP systems [7]. According to the mechanism, one of the two cation orbital states exists slightly below the chemical potential, and the other exists slightly above it. Then, a hybridization of the two orbitals substantiates the spin-dependent electron-hopping processes to

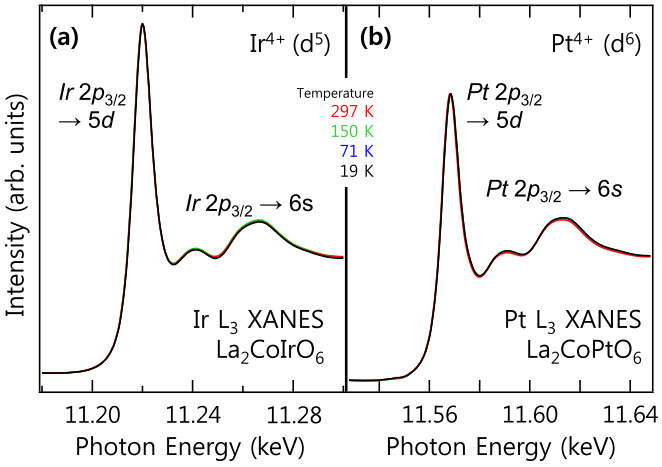

FIG. 5. T-dependent XANESs of (a) La_2CoIrO_6 and (b) La_2CoPtO_6 at Ir/Pt L_3 edges. The electronic structures of Ir/Pt $5d$ orbitals barely evolved with thermal disorders (with increasing T).

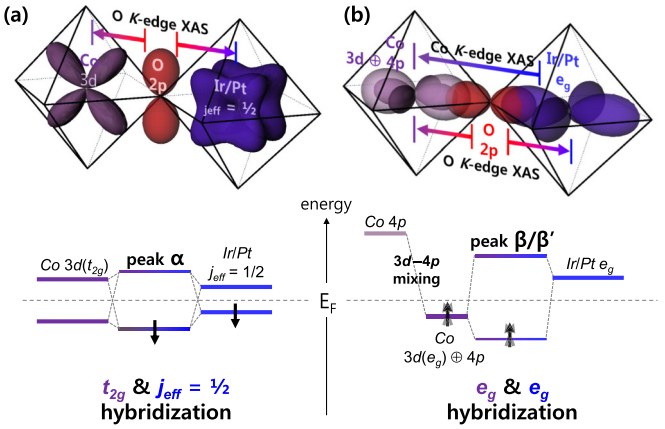

FIG. 6. Schematic diagrams of hybridized orbital states of (a) (Ir/Pt $5d$ $j_{\rm eff} = 1/2$)-(Co $3d$ t_{2g}) and (b) (Ir/Pt $5d$ e_g)-(Co $3d$ e_g that is mixed with Co $4p$). The unoccupied $5d$ e_g as well as the involvement of nonmagnetic Co $4p$ in the Co-O-Ir hybridization would not contribute to a spin ordering resulting in a paramagnetism, as is highlighted by the staggering spins in the energy level diagram in (b). The relevant spectroscopic techniques to observe the orbital hybridizations with peak assignments are also depicted.

stabilize either ferromagnetic or antiferromagnetic couplings between the TM-ion sublattices [3,4]. The nonlocal orbital hybridization enables the electron transfer (from B to B' ions in $A_2BB'O_6$) via the intermediate oxygen ions despite the long atomic distances between the two TM ions (~4 Å).

In the cases of La_2CoIrO_6 and La_2CoPtO_6, these hybridization processes can stabilize an antiferromagnetic ordering between Co $3d$ and Ir/Pt $5d$ spin states. Specifically, in order to invoke any effect on the electronic structures by intersite orbital hybridization, two orbitals (one is empty while the other is filled by an electron) should have identical symmetry. According to the limitation, there can be two possible channels of hybridization for $3d$ and $5d$ orbitals supported by intermediate oxygen: one is ($3d$ t_{2g})-($5d$ $j_{\rm eff} = 1/2$) through a π bonding, and the other is ($3d$ e_g)-($5d$ e_g) through a σ bonding, both of which are mediated by O $2p$ orbital states. The two hybridization configurations are depicted in the schematic diagrams (top panels) in Figs. 6(a) and 6(b), respectively. The relevant spectroscopies that can observe the orbital hybridizations are indicated as well.

The bottom panels in Fig. 6 show the schematic diagrams for the energy levels with the hybridization mechanism. Through the π bonding, the electrons from Co $3d$ t_{2g} can virtually hop to the unfilled Ir $5d$ $j_{\rm eff} = 1/2$, and likewise, the electrons from Ir $5d$ $j_{\rm eff} = 1/2$ can hop to the unfilled Co $3d$ t_{2g} [Fig. 6(a)]. According to a theoretical study on La_2CoIrO_6 [15], the electron hopping from Co t_{2g} to Ir $j_{\rm eff} = 1/2$ should play the dominant role in determining the ferrimagnetic order. Since the majority-spin states in Co^{2+} are completely filled, only hopping to the minority-spin states is allowed. The spin-selective process forces the Co and Ir spin states to be coupled antiferromagnetically to stabilize a ferrimagnetism in the iridate DP. The unfilled hybridized ($3d$ t_{2g})-($5d$ $j_{\rm eff} = 1/2$) state should account for peak α in the O K-edge XAS data. It is evident that an orbital hybridization between Co $4p$ and Ir/Pt $j_{\rm eff}$ states cannot exist due to the different parities for the space inversion symmetry. This can explain why peak α is almost absent in the Co K-edge XAS spectra (Co $1s \rightarrow 4p$).

Likewise, the electrons from Co e_g with majority spins can also hop to the unfilled Ir/Pt e_g states through the σ bonding [Fig. 6(b)]. However, since both the spin states of Ir/Pt e_g are empty (due to weaker Hund coupling effects compared to the case of $3d$ e_g), the virtual spin transfer from Co e_g to Ir/Pt e_g cannot induce any preference in the spin alignments between the Co and Ir/Pt sites. As a result, the presence of the $3d$ e_g–$5d$ e_g orbital hybridization will not contribute to the antiferromagnetic coupling.

The hybridized e_g–e_g orbital states were indeed observed as peaks β/β' in the O K-edge spectra (Fig. 2) and in the preedge regions of the Co K-edge spectra (Figs. 3 and 4). The observation of peaks β/β' through the Co $1s \rightarrow 4p$ transition is feasible due to $3d$–$4p$ intra-atomic orbital mixing due to slight distortions in BO_6.

B. Relevance of hybridized orbital states to the magnetism

The (Co $3d$ t_{2g})-(Ir/Pt $5d$ $j_{\rm eff} = 1/2$) hybridization mostly explains the stabilization of the antiferromagnetic coupling between the Co and Ir/Pt sublattices and the consequent ferrimagnetism in the iridate DP. However, this does not fully explain the peculiar magnetism of the Co^{2+} ions. It is shown in the previous x-ray magnetic circular dichroism (XMCD) measurement that, although ferromagnetic, the spin moment of Co is not saturated with increasing external magnetic field but continuously increases even up to 15 T [16]. This is in contrast to the Ir moment, which is readily saturated below 2 T. Moreover, our recent study showed that La_2CoIrO_6 and La_2CoPtO_6 also exhibited a persistent development in magnetization [17]. This implied that a certain paramagnetic contribution to the magnetic moment of Co ions is necessary to reach the ideal value of $+3\mu_B$.

As shown in Fig. 6, we propose that the hybridization of the Co $3d$ e_g orbitals with unpolarized Ir/Pt e_g orbitals additionally influences the magnetism in the $3d$–$5d$ DPs. From

the preedge structures in the Co K-edge XAS spectra and their T evolution (Figs. 3 and 4), we found that the Co $4p$-Ir/Pt e_g hybridization is strong and persistent even up to room temperature. The presence of the preedge peaks manifests that the Co $4p$ orbitals are partially filled by electrons, which can be accomplished only through the intra-atomic $3d-4p$ mixing. Co $4p$ orbitals tend to be mixed with Co $3d$ under a slight distortion of the octahedral CoO_6 coordination, so that part of the Co $4p$ becomes filled. This $3d-4p$ mixing process commonly appears in other TM octahedral as well, but it is usually not pointed out due to the small contribution to physical properties [35].

Owing to the partial filling of Co $4p$, the Co $4p$-Ir/Pt e_g hybridization can influence the electronic structure. As shown in Fig. 6(b), the $3d \oplus 4p$ states below the chemical potential can hybridize with the Ir/Pt e_g orbitals, which are not spin polarized. According to the hybridization mechanism in DPs, the ferromagnetic or antiferromagnetic coupling between B and B' spins is dictated by the spin-selective virtual electron-hopping process. Since the $5d$ e_g subshells are not spin polarized $[(e_g \uparrow)^2\ (e_g \downarrow)^2]$ due to the weak Hund coupling of the $5d$ orbitals, the $3d$ e_g-5d e_g hybridization will suppress the spin polarization of the Co $3d$ e_g. Therefore, we can tell that the (Co $3d$ $e_g \oplus 4p$)-(Ir/Pt $5d$ e_g) hybridization could serve as the origin of a paramagnetism against the antiferromagnetic ordering established by (Co $3d$ t_{2g})-(Ir $5d$ $j_{\rm eff} = 1/2$) hybridization. The possible involvement of unpolarized Co $4p$ orbitals in the hybridization might also contribute to the persistent paramagnetism observed in the iridate DP.

Therefore, the two intersite $3d(\oplus\ 4p)$-$5d$ hybridizations (with σ and π symmetries), described in Fig. 6, should be the key factors to determine the electronic structure and magnetism in the $3d-5d$ DPs. Particularly, the (Co $3d$ $e_g \oplus 4p$)-(Ir/Pt $5d$ e_g) hybridization, featured in this work, should not contribute to the antiferromagnetic intersite coupling but should serve as the origin of persistent paramagnetism in the iridate and platinate DPs. Meanwhile, in the case of well-known $3d-4d$ DPs, those intriguing spin interactions should be less prominent. This is because the Hund coupling in the $4d-e_g$ bands is strong, so the $3d$ e_g-4d e_g hybridization should be spin selective to contribute to a magnetic order. Therefore, the coexistence of the two functionalities, one constructive ($t_{2g}-j_{\rm eff}$) and the other almost inactive (e_g-e_g), of the magnetic order could be regarded as a peculiar property of the $3d-5d$ iridate or platinate DP.

V. CONCLUSION

From the O K-edge and Co K-edge XAS spectra of the iridate and platinate DPs, we observed two channels of orbital hybridizations. One is (Co $3d$ t_{2g})-(Ir/Pt $5d$ $j_{\rm eff} = 1/2$) with π bonding symmetry. This should be the primary origin of the stabilization of antiferromagnetic coupling between Co and Ir/Pt sublattices. The other is (Co $3d$ $e_g \oplus 4p$)-(Ir/Pt $5d$ e_g) with σ bonding symmetry. This should not contribute to the magnetic intersite coupling to induce paramagnetism competing with the dominant ferrimagnetism. The two functionalities persist far above the Curie temperature, suggesting their predominant roles in determining the magnetic structures in the iridate and platinate DPs.

ACKNOWLEDGMENTS

This work was supported by the Research Center Program of the Institute for Basic Science(IBS) in Korea (Grant No. IBS-R009-D1). D.-Y.C. acknowledges support from Basic Science Research Program through the National Research Foundation of Korea funded by the Ministry of Science, ICT & Future Planning (NRF-2015R1C1A1A02037514).

[1] R. Schlapp and W. G. Penney, Phys. Rev. **42**, 666 (1932).
[2] D. I. Khomskii, *Transition Metal Compounds* (Cambridge University Press, Cambridge, 2014).
[3] J. Kanamori and K. Terakura, J. Phys. Soc. Jpn. **70**, 1433 (2001).
[4] D. D. Sarma, P. Mahadevan, T. Saha-Dasgupta, S. Ray, and A. Kumar, Phys. Rev. Lett. **85**, 2549 (2000).
[5] H. Das, P. Sanyal, T. Saha-Dasgupta, and D. D. Sarma, Phys. Rev. B **83**, 104418 (2011).
[6] Y. Krockenberger, K. Mogare, M. Reehuis, M. Tovar, M. Jansen, G. Vaitheeswaran, V. Kanchana, F. Bultmark, A. Delin, F. Wilhelm, A. Rogalev, A. Winkler, and L. Alff, Phys. Rev. B **75**, 020404 (2007).
[7] D. Serrate, J. M. De Teresa, and M. R. Ibarra, J. Phys. Condens. Matter **19**, 23201 (2007).
[8] K.-I. Kobayashi, T. Kimura, H. Sawada, K. Terakura, and Y. Tokura, Nature (London) **395**, 677 (1998).
[9] B. J. Kim, H. Jin, S. J. Moon, J.-Y. Kim, B.-G. Park, C. S. Leem, J. Yu, T. W. Noh, C. Kim, S.-J. Oh, J.-H. Park, V. Durairaj, G. Cao, and E. Rotenberg, Phys. Rev. Lett. **101**, 076402 (2008).
[10] S. J. Moon, H. Jin, K. W. Kim, W. S. Choi, Y. S. Lee, J. Yu, G. Cao, A. Sumi, H. Funakubo, C. Bernhard, and T. W. Noh, Phys. Rev. Lett. **101**, 226402 (2008).
[11] G. Jackeli and G. Khaliullin, Phys. Rev. Lett. **102**, 017205 (2009).
[12] C. H. Sohn, H. Jeong, H. Jin, S. Kim, L. J. Sandilands, H. J. Park, K. W. Kim, S. J. Moon, D.-Y. Cho, J. Yamaura, Z. Hiroi, and T. W. Noh, Phys. Rev. Lett. **115**, 266402 (2015).
[13] C. H. Sohn, C. H. Kim, L. J. Sandilands, N. T. M. Hien, S. Y. Kim, H. J. Park, K. W. Kim, S. J. Moon, J. Yamaura, Z. Hiroi, and T. W. Noh, Phys. Rev. Lett. **118**, 117201 (2017).
[14] J. Chaloupka, G. Jackeli, and G. Khaliullin, Phys. Rev. Lett. **105**, 027204 (2010).
[15] N. Narayanan, D. Mikhailova, A. Senyshyn, D. M. Trots, R. Laskowski, P. Blaha, K. Schwarz, H. Fuess, and H. Ehrenberg, Phys. Rev. B **82**, 024403 (2010).
[16] A. Kolchinskaya, P. Komissinskiy, M. B. Yazdi, M. Vafaee, D. Mikhailova, N. Narayanan, H. Ehrenberg, F. Wilhelm, A. Rogalev, and L. Alff, Phys. Rev. B **85**, 224422 (2012).

[17] M.-C. Lee, C. H. Sohn, S. Y. Kim, K. D. Lee, C. J. Won, N. Hur, J.-Y. Kim, D.-Y. Cho, and T. W. Noh, J. Phys. Condens. Matter **27**, 336002 (2015).
[18] J. Song, B. Zhao, L. Yin, Y. Qin, J. Zhou, D. Wang, W. Song, and Y. Sun, Dalton Trans. **46**, 11691 (2017).
[19] L. T. Coutrim, D. C. Freitas, M. B. Fontes, E. Baggio-Saitovitch, E. M. Bittar, E. Granado, P. G. Pagliuso, and L. Bufaiçal, J. Solid State Chem. **221**, 373 (2015).
[20] B. Ranjbar, E. Reynolds, P. Kayser, B. J. Kennedy, J. R. Hester, and J. A. Kimpton, Inorg. Chem. **54**, 10468 (2015).
[21] J.-H. Sim, H. Yoon, S. H. Park, and M. J. Han, Phys. Rev. B **94**, 115149 (2016).
[22] E. Kermarrec, C. A. Marjerrison, C. M. Thompson, D. D. Maharaj, K. Levin, S. Kroeker, G. E. Granroth, R. Flacau, Z. Yamani, J. E. Greedan, and B. D. Gaulin, Phys. Rev. B **91**, 075133 (2015).
[23] A. E. Taylor, R. Morrow, D. J. Singh, S. Calder, M. D. Lumsden, P. M. Woodward, and A. D. Christianson, Phys. Rev. B **91**, 100406 (2015).
[24] A. E. Taylor, S. Calder, R. Morrow, H. L. Feng, M. H. Upton, M. D. Lumsden, K. Yamaura, P. M. Woodward, and A. D. Christianson, Phys. Rev. Lett. **118**, 207202 (2017).
[25] P. Kayser, S. Injac, B. J. Kennedy, T. Vogt, M. Avdeev, H. E. Maynard-Casely, and Z. Zhang, Inorg. Chem. **56**, 6565 (2017).
[26] C. M. Thompson, L. Chi, J. R. Hayes, A. M. Hallas, M. N. Wilson, T. J. S. Munsie, I. P. Swainson, A. P. Grosvenor, G. M. Lukebe, and J. E. Greedanab, Dalton Trans. **44**, 10806 (2015)
[27] H. Kato, T. Okuda, Y. Okimoto, Y. Tomioka, Y. Takenoya, A. Ohkubo, M. Kawasaki, and Y. Tokura, Appl. Phys. Lett. **81**, 328 (2002).
[28] A. L. Ankudinov, B. Ravel, J. J. Rehr, and S. D. Conradson, Phys. Rev. B **58**, 7565 (1998).
[29] F. M. F. de Groot, M. Grioni, J. C. Fuggle, J. Ghijsen, G. A. Sawatzky, and H. Petersen, Phys. Rev. B **40**, 5715 (1989).
[30] J. Suntivich, W. T. Hong, Y. Lee, J. M. Rondinelli, W. Yang, J. B. Goodenough, B. Dabrowski, J. W. Freeland, and Y. Shao-Horn, J. Phys. Chem. C **118**, 1856 (2014).
[31] P. A. Lee, P. H. Citrin, P. Eisenberger, and B. M. Kincaid, Rev. Mod. Phys. **53**, 769 (1981).
[32] J. J. Rehr and R. C. Albers, Rev. Mod. Phys. **72**, 621 (2000).
[33] F. de Groot, G. Vanko, and P. Glatzel, J. Phys.: Condens. Matter **21**, 104207 (2009).
[34] D. Cabaret, A. Bordage, A. Juhin, M. Arfaoui, and E. Gaudry, Phys. Chem. Chem. Phys. **12**, 5619 (2010).
[35] T. E. Westre, P. Kennepohl, J. G. DeWitt, B. Hedman, K. O. Hodgson, and E. I. Solomon, J. Am. Chem. Soc. **119**, 6297 (1997).